Modelling the Enthalpy change and Transition Temperature dependence of the Metal-Insulator Transition in Pure and Doped Vanadium Dioxide

Haichang Lu[1], Stewart Clark[2], Yuzheng Guo[1, 3] and John Robertson[1]*

[1]Department of Engineering, Cambridge University, Cambridge CB2 1PZ, United Kingdom
[2]Department of Physics, Durham University, Durham DH1 3LE, United Kingdom
[3]School of Electrical Engineering and Automation, Wuhan University, Wuhan, China
*Email: yg262@cam.ac.uk

We compare various calculation methods to determine the electronic structures and energy differences of the phases of VO_2. We show that density functional methods in the form of GGA+U are able to describe the enthalpy difference (latent heat) between the rutile and M_1 phases of VO_2, and the effect of doping on the transition temperature and on the band gap of the M_1 phase. An enthalpy difference of ΔE_0= -44.2meV per formula unit, similar to the experimental value, is obtained if the randomly oriented spins of the paramagnetic rutile phase are treated by a non-collinear spin density functional calculation. The predicted change in the transition temperature of VO_2 for Ge, Si or Mg doping is calculated and is in good agreement with the experiment data.

I. INTRODUCTION

Vanadium Dioxide (VO_2) has a first-order metal-insulator transition (MIT) at around 340K between its high-temperature metallic rutile (R) phase and a low-temperature semiconducting monoclinic (M_1) phase [1] which make it of great interest for applications such as smart window materials, Radio Frequency (RF) or optical switches, sensors [2-6], or as the channel material in steep-slope field effect transistors (FETs) [7-10] using the 'Mott-FET' concept [11]. To develop these applications, it is useful to be able to vary the transition temperature T_c, and the band gap of the insulating phase by doping, and to be able to calculate these properties suitable for use in appropriate device models. For each of these uses, it would be advantageous to have a fast but reliable computational method to describe the electronic structure and phase energetics that can be extended to large supercells of several hundred atoms or more.

Three results of an electronic structure calculation are of interest, (1) the atomic and spin configurations, (2) the band structure or density of states, and (c) the free energy differences between the phases. Here, we are particularly interested in the free energy differences between the phases as these are important for modeling the on/off voltages of electronic devices [7-9]. On the other hand, many groups are highly interested in trying to separate the electronic and structural components of the phase transition by time scales [12,13], but this is of less concern here.

Correlated materials like VO_2 are known to require electronic structure methods that go beyond density functional theory (DFT) [14], such as cluster dynamic mean field theory (c-DMFT), GW or quantum Monte-Carlo [15-18]. However, these methods are computationally demanding. On the other hand, efforts to use the less computationally demanding local density approximation (LDA) to describe VO_2 were deemed a failure because it gave no band gap for the insulating M_1 phase [19].

There are two less demanding methods which can introduce a band gap; applying a Hubbard potential U to the transition metal 3d orbitals as in the classic case of NiO [20], or by using hybrid functionals [21-23]. The LDA+U method has been used previously on VO_2 by various authors [24]. It was also further developed into the cluster DMFT method [16].

The second less demanding method of hybrid functionals adds a fraction (α) of non-local Hartree-Fock (HF) exchange to the semi-local density exchange-correlation function. This can correct the DFT band gap error for a wide range of molecules, semiconductors and insulators, whether they are s, p bonded or d-electron materials. Typically, these methods add α=25% of HF exchange to the local density functional [21-23]. Eyert [25,26] found that the Heyd-Scuseria-Ernzerhof (HSE) hybrid functional [22] provides a band gap for the VO_2 M_1 phase.

However, Grau-Crespo et al [27,28] criticized the hybrid functional approach by noting that HSE greatly over-estimated the enthalpy difference between R and M_1 phases compared to the experimental values of Navrotsky et al [29] and Berglund et al [30]. This would translate to a large error in any modeling of FET characteristics. We find that the main error was a mis-calculation of the enthalpy of the R phase. We also note that hybrid functional methods do over-estimate the latent heats, but that this problem can be reduced by using lower fractions of HF admixture, as others noted [31-33]. The second objective of this paper is to derive how specific alloying will change the band gap and transition temperature T_c.

II. METHODS

The calculations are carried out using both the electronic structure programs VASP [34] and supported by CASTEP [35], with a plane-wave basis set converged to 10^{-6} eV per atom. The exchange-correlation functional is the Perdew-Burke-Ernzerhof (PBE) form of the generalized gradient approximation (GGA), applying an on-site U potential for the vanadium d-electrons to augment the Coulomb repulsion. GGA+U is a computationally convenient method to compensate the band gap error. The rotationally invariant Liechtenstein's form of GGA+U [36] (U = 2.0 eV and J= 0.3 eV) was adopted to match the experimental gap [37]. The same U value is used for both R and M_1 phases.

We construct the primitive cell of the monoclinic M_1 phase by doubling the primitive cell of the rutile phase along z-direction [38], as shown in Fig. 1. The R and M_1 structures are from ref [38], together with the magnetism and exchange couplings shown in Fig. 1.

The rutile phase can only be modeled by a supercell containing many primitive cells, in order to represent the orientation disorder of spins in this paramagnetic (PM) phase. For the PM supercells, we generate a random direction for each magnetic moment of V using the spin-orbital coupling package, with zero initial net magnetic moments in each direction with the initial magnitude of each moment of vanadium set to 1. We then use a non-collinear spin DFT (NCS-DFT) calculation of the CASTEP or VASP codes. The random spins are then relaxed within the self-consistent energy calculation to an energy minimum. The magnitude of each spin stays at 1. We average over several different PM runs. The internal atomic coordinates are relaxed until the residual force is less than 0.03eV/Å.

The experimental atomic coordinates are used for the R and M_1 structures, as shown in Fig 1(b) [39]. A spin dimerized V-V geometry of the M_1 structure is obtained, with V-V separations of 2.65Å and 3.12Å along the chain. These give a greater variation of the V-V distance than do relaxed GGA+U calculations. We use 5x5x5 k-points for M_1 and small size R cells, and 2x2x2 k-points for R supercells with 108 VO_2 units (324 atoms) and 256 VO_2 units (768 atoms), converging energy differences to around 10^{-6} eV per atom.

III RESULTS

A. Latent heat in VO_2

The spin ordering in the M_1 phase is described as non-magnetic singlet state consisting of spin dimers with strong intra-dimer coupling, along the V-V chains in the Oz direction, by

Zheng and Wagner [17] and shown in Fig 1(b). The experimental V-V separations are 2.65Å and 3.12Å [39]. The V-V dimers give a weak temperature-independent van Vleck paramagnetic susceptibility as found by Kosuge [40] and Pouget [41]. However, our GGA+U relaxation gives a weaker dimerization, with calculated distances of 2.864 Å and 2.889 Å. This leads to the spin state being described as antiferromagnetic in many DFT calculations.

The total energy differences are shown in Fig. 2. The difference in total energies per formula unit in the M_1 and paramagnetic R phases, ΔE_0, converges to a latent heat of -44.2 meV for a large number of cells, as seen in Fig 2(a). This is close to the experimental value.

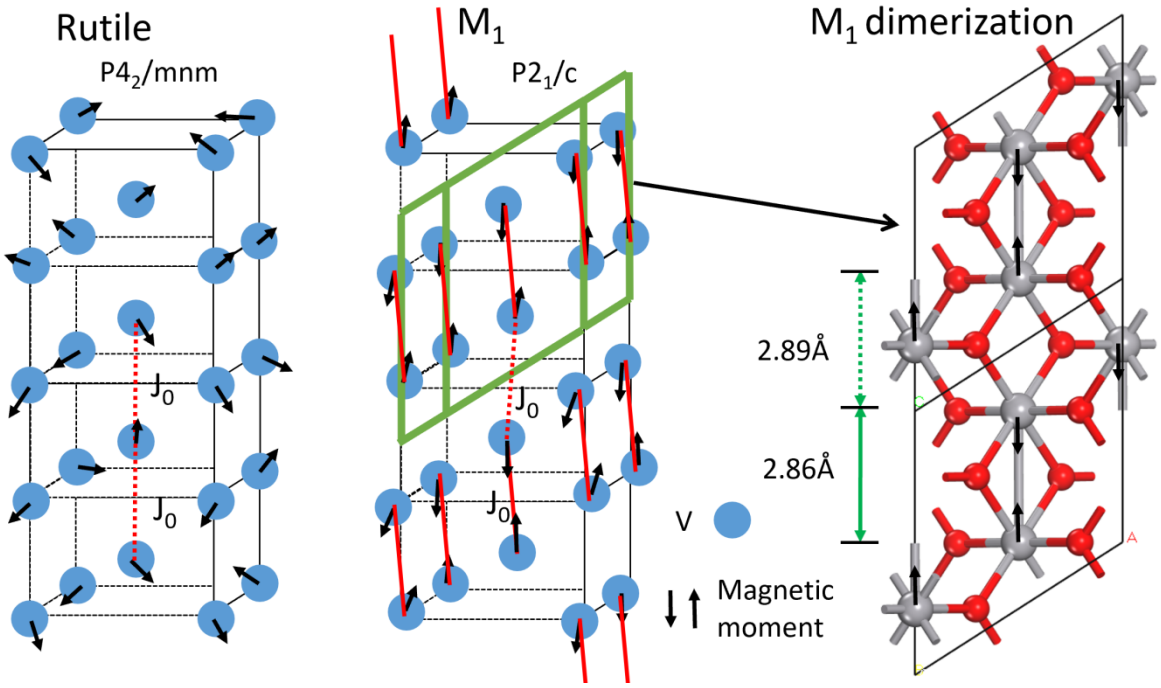

Figure. 1(a) Atomic structure and magnetic moments of VO_2 in the high temperature (rutile) and low temperature (M_1) phases. The primitive cell of rutile is shown in thin black lines, the primitive cell of M_1 of two rutile cells is shown by thick green lines. (O atoms are not shown for clarity.) (b) M1 lattice. Two primitive cells of M_1 are used to show the V-V dimerization. Relaxed V-V separations are shown.

Fig. 2(b) shows that *s*, the average spin per dimer in the PM phase, decreases as the number of V atoms in the cell increases, as shown pictorially in Fig. 2(c). In FM, *s*=1, while for PM, *s* should be zero. As a result, a supercell with more than 32 VO_2 units is suitable to describe the PM state, which is consistent with Fig. 2(a). The partial density of states (PDOS) of the R and M_1 phases is shown in Fig. 2(d). A gap of 0.6eV is obtained for M_1, which is close to the experimental band gap [32]. The band edge of monoclinic VO_2 is made of unpaired d electrons of vanadium. For each dimer, there is one occupied d band and nine empty d bands, so one unpaired electron occupies each V site, which is mainly d_z^2 ($d_{//}$) orbital. For the PM rutile supercell, we use the result of 72 VO_2 units which is sufficiently PM, the $d_{//}$ and π^* bands are both partially filled.

As noted, Grau-Crespo et al [28] criticized hybrid functionals for over-estimating the latent heat of the transition. However these authors took the R phase to be non-magnetic (NM), whereas experimentally Kosuga [40] and Pouget [41] found this phase to be paramagnetic (PM). Thus, each vanadium atom in the R phase carries a spin of $1\mu_B$ pointing in a random

direction. This spin ordering and non-collinear spin-polarized GGA+U density functional calculation using large supercells give a latent heat close to experiment.

Nuclear magnetic resonance (NMR) and electron spin resonance (EPR) found that VO_2 is indeed a correlated oxide with a magnetic moment 1 μ_B on each vanadium atom [41-43]. Huffmann et al [37] argued that as the M_1, M_2 and T phases have the same d-d optical peak at 2.5 eV, despite their different V-V dimerization patterns, while a Peierls model would give different energies, so this favors a Mott insulator description of the band gap of M_1.

The heat of formation of the PM phase is also calculated approximately with the HSE functional, a more expensive calculation than GGA+U, but for a small cell of four VO_2 units. Interestingly, the latent heat is quite close to the experimental value even for α=0.1 and α=0.25 HF fraction, consistent with it being composed mainly of entropy contributions [44,45]. Thus varying α or U affects mainly the relative stability of NM and FM states, not the PM vs AFM difference, as seen in Fig 3(c), except at very low values of α where FM phases appear. The HSE is expected to give similar results to GGA+U by choosing the proper α, but it is more time-consuming. It is interesting that one of the first hybrid functionals, B3LYP, fits the band gap of most s.p semiconductors *and* the correlated oxide NiO [24] with α = 25%, but VO_2 does not seem to fit within this scheme [32].

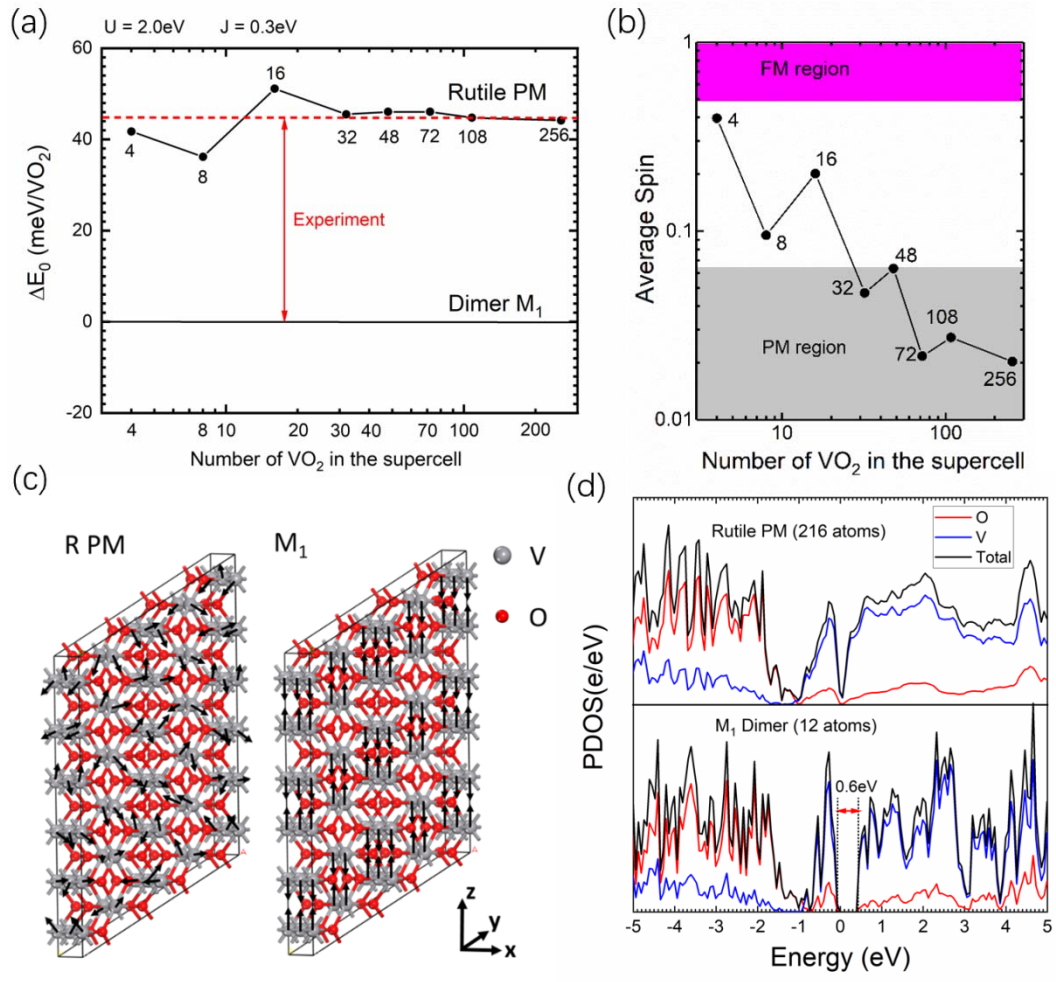

Figure 2. (a) The calculated latent heat ΔE_0 for the MIT vs supercell size. The experimental latent heat is marked by the red dashed line. The number of VO_2 units per supercell is marked near the black dots. (b) average spin per dimer in the PM phase vs. the number of VO_2 units per supercell. (c) Schematic of atomic structures and magnetic order of pure VO_2 in PM rutile and AFM M_1 phases, 144 atoms. (d) Electronic density of states in R and M_1 phases.

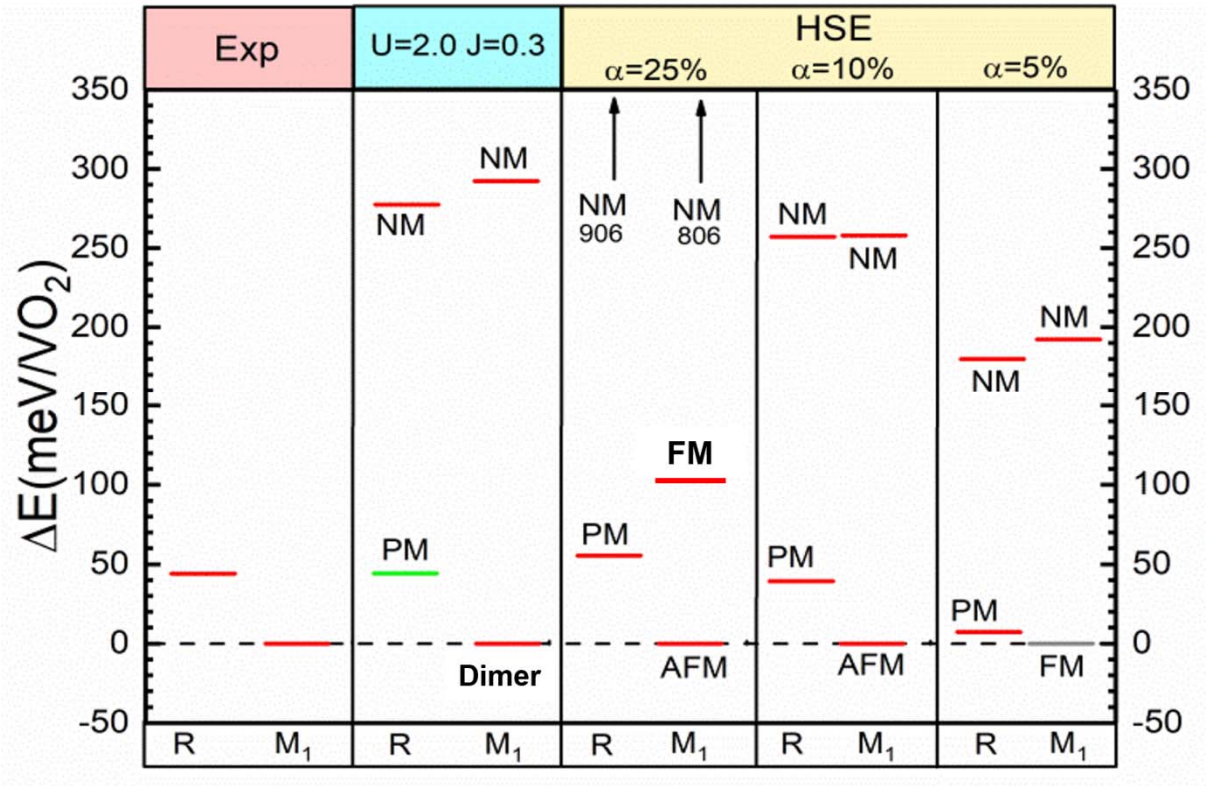

Figure 3. (a) Experimental heats of formation/VO_2 unit; (b) GGA+U heat of formation, showing latent heat between PM (R) and dimer (M_1) phase; (c) HSE version according to Grau-Crespo with mis-assigned NM states and HSE energies for PM R, and AFM M_1 phases for other fractions of HF.

B. Transition temperature

The Heisenberg Hamiltonian can be used to describe the chains of V spins, and it can be written as

$$\hat{H} = -\frac{1}{2}\sum_{i\neq j} J(r_{ij})\hat{s}_i\hat{s}_j \qquad (1)$$

where J is the exchange coupling between the i and j pairs of V atoms. J<0 if AFM is energetically favored, $\hat{s}_i$ is the spin of the i^{th} V. The exchange coupling between vanadium atoms decays roughly as $J(r_{ij}) \propto r_{ij}^{-3}$ due to dipolar interactions in an insulating phase, and decays more rapidly in metals. Therefore, exchange between more distant vanadium atoms is negligible so we show only intra-chain J_0, J_1, J_2 and inter-chain J_0', J_1', J_2' interactions in Fig 1(a). Therefore the system can be considered to be made of V-V dimers, and the Heisenberg dimer model gives

$$\hat{H} = -J_0\hat{s}_1\hat{s}_2 = -\frac{1}{2}J_0[(\hat{s}_1+\hat{s}_2)^2 - \hat{s}_1{}^2 - \hat{s}_2{}^2] = -\frac{1}{2}J_0[\hat{s}^2 - \frac{3}{2}] \qquad (2)$$

where $\hat{s}_1$ and $\hat{s}_2$ are the spin of two closest V, $\hat{s}$ is the total spin, $\hat{s}^2 = s(s+1)$, s=1 is the triplet state (FM), s=0 is the singlet state (AFM). The singlet energy is -¾$|J_0|$, while the triplet energy is ¼$|J_0|$. Then $|J_0|$ is the singlet-triplet excitation energy.

This allows us to calculate J_0= -58.9meV or from the latent heat by using

$$\Delta E_0 = \frac{3}{4}J_0 \qquad (3)$$

The transition temperature T_C can be derived from mean-field theory [46,47] as:

$$T_C = \frac{2S(S+1)}{3k_B}(-J_0) \qquad (4)$$

where S=½ which gives T_C = 341.9K.

Thus, we can obtain the transition temperature of pure VO_2 from the latent heat.

C. Doped VO_2 and their transition temperatures

The transition temperature of VO_2 can be varied by doping. The MIT in the alloys happens in the same way as in pure VO_2. We replace a V atom with a dopant in the supercell of 48 VO_2 units for 2.08% doping and in the supercell of 32 VO_2 units for 3.125% doping and two isolated V atoms for 6.25% doping [38]. The relaxed structures and schematic spin configurations are shown in Fig. 4(a). We choose Ge, Mg and Si as the dopants as they are non- magnetic, in order to use eqn (2) for T_C. For Mg, O vacancies are also required to maintain valence satisfaction, which modifies the V network to give V coordinations of 5 for higher alloying ratios in those cases. The overall atomic configurations and electronic and spin structures were given earlier [38]. The PDOS of a sample with 2.08% Ge doping is shown in Figs. 4(b).

The transition temperature of X-doped (X=Ge, Mg, Si) VO_2, $T_{C,X}$, can be scaled from the T_C of the pure VO_2. The energy change of X-doped VO_2 represents the overall exchange coupling (noting that the dopants are sufficiently far away from each other),

$$\Delta E_X = \frac{E_{AFM}-E_{PM}}{N} = \frac{3}{4}J_{0,X}(1-n) \qquad (5)$$

where n is the doping ratio and where N is the number of formula units of VO_2. The T_C of X-doped VO_2 can be written as

$$T_{C,X} = T_C \frac{\Delta E_X}{\Delta E_0(1-n)} \qquad (6)$$

Fig. 4(c) shows the calculated and experimentally measured [49-51] transition temperatures of doped VO_2. Fig. 4(d) shows the band gap of doped VO_2. It is interesting that all three dopants reduce the band gap of the M_1 phase, while Ge and Si raise T_C and Mg lowers it, in both experiment and theory. To raise the gap, it is necessary for Mg doping to create the M_2 phase with a different V coordinations, which it does at higher doping concentrations [38]. The band gap and Tc values do not vary monotonically for Mg alloys because of changes in the atomic configuration of its alloys.

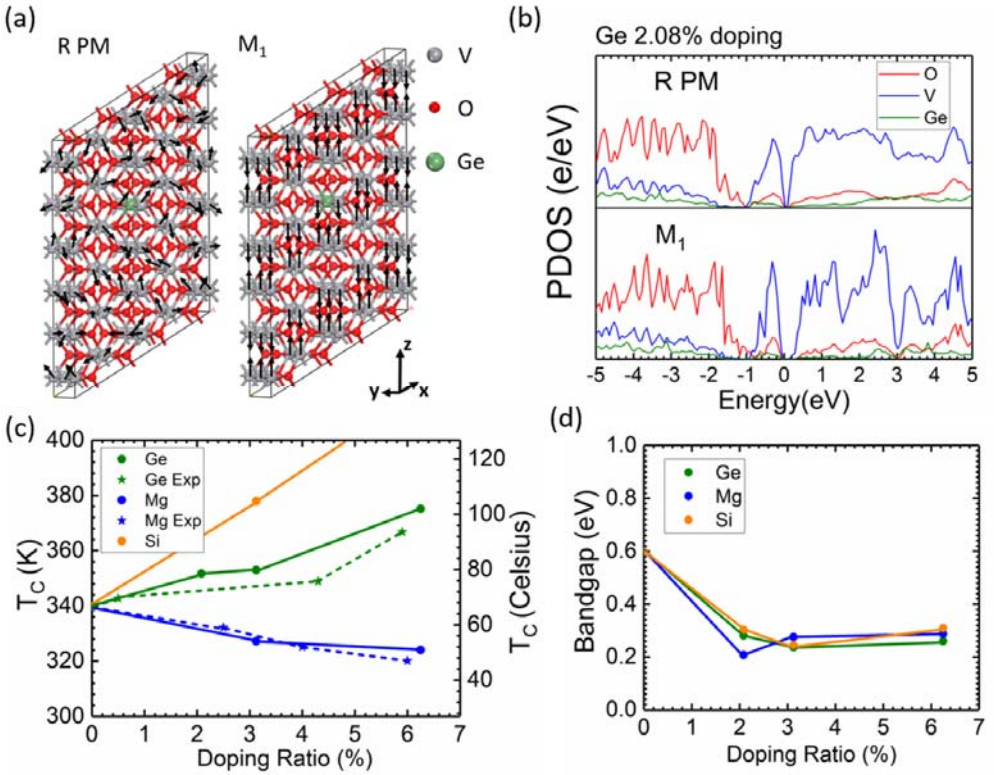

Figure 4. (a) The atomic structure and the schematic spin order of the HT and the LT phase of the 2.08% doped VO_2, and their PDOS (b). (c) Transition temperature vs Ge, Si and Mg doping ratio, the dashed lines are from experiments [49-51]. (d) Band gaps of Ge, Si and Mg doped VO_2.

In conclusion, we have carried out DFT calculations on pure and doped VO_2 to illustrate the nature of its MIT. A Hubbard U term is added to correct the Coulomb repulsion in this strongly-correlated system. The method is less computational demanding than using the hybrid functionals, DMFT or GW but is able to produce robust results. We identify the magnetic ground state of the HT phase as PM and the LT phase as effectively AFM. The band gap arises from a spin-alignment. The latent heat of transition is calculated by fully representing the non-collinear magnetic ordering of the paramagnetic rutile phase. The Ge-doped VO_2 is also calculated. The band gap of Ge doped VO_2 is decreased compared to pure VO2. The transition temperature of Ge doped VO_2 increases. These results are consistent with experiment. This paper sheds new light on the long-term debated topic and solves the total energy problem, which confirms that magnetic ground state transition plays a crucial role in MIT.

We acknowledge the European Commission H2020 grant (Phase-change switch), Cambridge University's Skylake Facilities, the Archer Supercomputer, Wuhan University Supercomputer and Durham University's Hamilton HPC facilities.

References

1. F. J. Morin, *Phys. Rev. Lett.* **3**, 34 (1959).
2. K. Liu, S. Lee, S. Yang, O. Delaire, J. Wu, *Materials Today* **21**, 875 (2018**)**.
3. S. Wang, M. Liu, L. Kong, Y. Long, X. Jiang and A. Yu, *Prog. Mater Sci.* **81**, 1-54 (2016**).**
4. P. Markov, R. E. Marvel, H. J. Conley, K. J. Miller, R. F. Haglund, Jr. and S. M. Weiss, *ACS Photonics* **2**, 1175-1182 (2015**)**.
5. W. A. Vitale, L. Petit, C. F. Moldovan, M. Fernandez, A. Paone, A. Schuler and A. M. Ionescu, *Sensors Actuators A: Physical* **241**, 245 (2016).
6. E. A. Casu, N. Oliva, M. Cavalieri, A. A. Muller, A. Fumarola, W. A. Vitale, A. Krammer, A. Schüler, M. Fernandez and A. M. Ionescu, *IEEE J EDS* **6**, 965 (2018); E. Corti, A. Khanna, K. Niang, J. Robertson, K. E. Moselund, B. Gotsmann, S. Datta and S. Karg, *IEEE EDL* **41**, 629 (2020).
7. Z. Yang, C. Ko and S. Ramanathan, *Ann. Rev. Mater. Res.* **41**, 337 (2011)
8. N. Shukla, A. V. Thathachary, A. Agrawal, H. Paik, A. Aziz, D. G. Schlom, S. K. Gupta, R. Engel-Herbert and S. Datta, *Nat. Communication* **6**, 7812 (2015).
9. T. Yajima, T. Nishimura and A. Toriumi, *Nat. Comm*unication **6** 10104 (2015).
10. T Yajima, T Nishimura and A Toriumi, *Small* **13**, 1603113 (2017).
11. C. Zhou, D. M. Newns, J. A. Misewich and P. C. Pattnaik, *Appl. Phys. Lett.* **70**, 598 (1997).
12. D. Wegkamp, M. Herzog, L. Xian, M. Gatti, P. Cudazzo, C. L. McGahan, R. E. Marvel, R. E. Hagland, A. Rubio, M. Wolf and J. Stahler, *Phys. Rev. Lett.* **113**, 216401 (2014).
13. A. Cavalleri, T. Dekorsy, H. H. W. Chong, J. C. Kieffer, R. W. Schoenlein, *Phys. Rev. B* **70**,161102 (2004)
14. R. M. Wentzcovitch, W. W. Schulz and P. B. Allen, *Phys. Rev. Lett.* **72**, 21 (1994)
15. S. Biermann, A. Poteryaev, A. I. Lichtenstein and A. Georges, *Phys. Rev. Lett.* **94**, 026404 (2005).
16. M. Gatti, F. Bruneval, V. Olevano and L. Reining, *Phys. Rev. Lett.* **99**, 266402 (2007).
17. H. Zheng and L. K. Wagner, *Phys. Rev. Lett.* **114**, 176401 (2015).
18. T. C. Koethe, Z. Hu, M. W. Haverkort, C. Schüßler-Langeheine, F. Venturini, N. B. Brookes, O. Tjernberg, W. Reichelt, H. H. Hsieh, H. J. Lin, C. T. Chen and L. H. Tjeng, *Phys. Rev. Lett.* **97**, 116402 (2006).
19. J. P. Pouget, H. Launios, J. P. Dhaenens, P. Merenda and T. M. Rice, *Phys. Rev. Lett.* **35**, 873 (1975).
20. V. I. Anisimov, J. Zaanen, O. K. Andersen, *Phys. Rev. B* **44**, 943 (1991). NiO
21. A. D. Becke, *J. Chem. Phys.* **98**, 5648 (1993).
22. J. Heyd, G. E. Scuseria and M. Ernzerhof, *J. Chem. Phys.* **118**, 8207 (2003).
23. J. Muscat, A. Wander and N. M. Harrison, *Chem. Phys. Lett.* **342**, 397 (2001).
24. A. Liebsch, H. Ishida and G. Bihlmayer, *Phys. Rev. B* **71**, 085109 (2005).
25. V. Eyert, *Phys. Rev. Lett.* **107**, 016401 (2011).
26. V. Eyert, *Annal. Phys.* **11**, 650 (2011).
27. R. Grau-Crespo, H. Wang and U. Schwingenschlögl, *Phys. Rev. B* **86**, 081101 (2012**)**.
28. H. Wang, T. A. Mellan, R. Grau-Crespo and U. Schwingenschlögl, *Chem. Phys. Lett.* **608**, 126 (2014**)**.
29. F. Pintchovski, W. S. Glaunsinger and A. Navrotsky, *J. Phys. Chem. Solids* **39**, 941-949 (1978**)**.
30. C. N. Berglund and H. J. Guggenheim, *Phys. Rev.* **185**, 1022 (1969).
31. F. Iori, M. Gatti and A. Rubio, *Phys. Rev. B* **85**, 115129 (2012);
32. X. Yuan, Y. Zhang, T. A. Abtew, P. Zhang and W. Zhang, *Phys. Rev. B* **86**, 235103 (2012)
33. B Xiao, J Sun, A Ruzsinszky, J P Perdew, Phys Rev B 90 085134 (2014)
34. G. Kresse, J. Furthmüller, *Phys. Rev. B* **54**, 11169 (1996); G. Kresse, J. Furthmüller, *Comput. Mater. Sci.* **6**, 15 (1996).
35. S. J. Clark, et al, Zeit. fur Krystall.. **220**, 567 (2005). DOI: 10.1524/zkri.220.5.567.65075; A. DalCorso, A. M. Conte, *Phys. Rev. B* **71**, 115106 (2005)
36. A. I. Liechtenstein, V. I. Anisimov, J. Zaane, *Phys. Rev. B* **52**, R5467 (1995).
37. H. Lu, Y. Guo and J. Robertson, *Phys. Rev. Mater.* **3**, 094603 (2019).
38. T. J. Huffman, C. Hendriks, E. J. Walter, J. Yoon, H. Ju, R. Smith, G. L. Carr, H. Krakauer and M. M. Qazilbash, *Phys. Rev. B* **95**, 075125 (2017).
39. A Magneli, G Andersson, Acta Chem Scan 9 1378 (1955); J Longo, P Kierkegaard, Acta Chem Scan 24 420 (1970)
40. K. Kosuge, *J. Phys. Soc. Jpn.* **22,** 551 (1967).
41. J. P. Pouget, H. Launios, T. M. Rice, P. Dernier, A. Gossard, G. Villeneu, P. Hagenmuller, *Phys. Rev. B* **10**, 1801 (1974).
42. J. P. Dhaenens, D. Kaplan and P. Merenda, *J. Phys. C* **8**, 2267 (1975).
43. J. P. Pouget, P. Lederer, D. S. Schreiber, H. Launois, D. Wohllebel, A. Casalot, G. Villaneuve, *J. Phys. Chem. Solids* **33**, 1961 (1972).
44. T. A. Mellan, H. Wang, U. Schwingenschlogl, R. Grau-Crespo, *Phys. Rev. B* **99**, 064113 (2019).
45. J. D. Budai, J. Hong, M. E. Manley, E. D. Specht, A. H. Said, B. Lieu, L. A. Boatner, R. McQueeny and O. Delaie, *Nature* **515**, 535 (2014).
46. C. Kittel, *Introduction to Solid State Physics, (7th ed, Wiley)* p446.
47. M. Netsianda, P. E. Ngoepe, C. R. A. Catlow, S. M. Woodley, *Chem. Mater.* **20**, 1764(2008).
48. A. Krammer, A. Magrez, W. A. Vitale, P. Mocny, P. Jeanneret, E. Guibert, H. J. Whitlow, A. M. Ionescu and A. Schüler, *J. Appl. Phys.* **122**, 045304 (2017**)**.
49. A. Krammer, OP. Bouvard and A. Schüler, *Energy Procedia*, **122**, 745-750 (2017).
50. N. R. Mlyuka, G. A. Niklasson and C. G. Granqvist, *Appl. Phys. Lett.* **95**, 171909 (2009).